New Sensorless Vector Control System With High Load Capacity Based on Improved SMO and Improved FOO

WENQI LU[1], (Member, IEEE), DONGYANG ZHENG[1], YUJUN LU[1],
KAIYUAN LU[2], (Member, IEEE), LIANG GUO[1], WEICAN YAN[3,4], AND JIAN LUO[5]

[1]Faculty of Mechanical Engineering and Automation, Zhejiang Sci-Tech University, Hangzhou 310018, China
[2]Department of Energy Technology, Aalborg University, DK-9220 Aalborg, Denmark
[3]Department of Electrical Engineering, Zhejiang University, Hangzhou 310018, China
[4]Wolong Electric Group Company Ltd., Shaoxing 312300, China
[5]Maider Medical Industrial Equipment Company Ltd., Taizhou 317600, China

Corresponding authors: Wenqi Lu (luwenqi@zstu.edu.cn) and Kaiyuan Lu (klu@et.aau.dk)

ABSTRACT In the existing sensorless vector control system of permanent magnet synchronous motor (PMSM), direct differential calculation or phase-locked loop (PLL) control is often used to estimate the rotor speed, but this method has some problems of weak load capacity and slow dynamic response. A new sensorless vector control method based on an improved sliding mode observer (SMO) and improved full-order observer (FOO) is proposed in this paper. The cut-off frequency of the low-pass filter is designed as a function of speed, the back EMF is fed back into the stator current estimation mathematical model, and the adaptive rate of feedback gains coefficient is proposed for improving the traditional SMO. The disturbance feedback matrix is introduced for improving the traditional FOO, and the estimated load torque is feedforward compensated to the given end of the quadrature current. An integrated system of corresponding algorithms is established, a test platform is built. The experimental results show that the speed and load torque estimation performance of the improved observer is better than that of the traditional observer in the process of sudden load change. The sensorless vector control system based on the proposed observer has a high dynamic response, load capacity, and reliability.

INDEX TERMS Sensorless vector control system, improved sliding mode observer (SMO), improved full-order observer (FOO), load capacity, reliability.

I. INTRODUCTION

The sensorless vector control system of permanent magnet synchronous motor (PMSM) has the advantages of simple structure, easy maintenance, small size, no limitations brought by mechanical sensors to the system (such as working environment limitations, reliability reduction, etc.) [1]. It can be applied to some special occasions, such as compressor [2], [3], water pump [4], [5], washing machine [6], etc. The effective estimation of the rotor position and velocity information is one of the critical technologies for the sensorless vector control system. And the performance of the control system depends on the accuracy, dynamic response,

and reliability of the information estimation. At present, according to the scope of application, there are two common estimation methods, among which the methods in [7]–[10] are suitable for zero low-speed operation, and the methods in [11]–[16] and [23]–[29] are suitable for medium high-speed operation.

For zero-low speed, in [7], [8], a high-frequency injection method is used to detect the rotor position of the motor and realize the rotor position estimation at low speed, including zero speed. However, this method will introduce high-frequency noise in specific applications, which applies to salient pole PMSM. In [9], [10], the voltage pulses vector method is used to detect the initial position of the motor at zero speed, and this algorithm is simple to implement. But with the applied voltage vector approaching the actual

The associate editor coordinating the review of this manuscript and approving it for publication was Hai Wang[ID].

rotor position, the difference of current response amplitude gradually decreases, which makes it more difficult to judge the amplitude. Therefore, the position estimation accuracy of this method is limited.

For medium-high speed, in [11], [12], the Luenberger observer is used to estimate the rotor position, whose results show that the ideal estimation effect can be obtained at low, medium, and high speeds. But it needs an independent filtering link, which increases the difficulty and workload in the system design and debugging process. In [13], [14], the model reference adaptive control (MRAC) is used to estimate the rotor position. This algorithm severs the actual motor model as the reference model and takes the flux linkage model as the adjustable model. According to the output error between the models and the corresponding adaptive law, the rotor position can be effectively estimated with high accuracy. However, the algorithm is relatively complex and easily affected by motor parameters, it has a greater impact on the performance of the rotor position following, which in turn makes the system dynamic response performance and reliability poor. In [15], [16], the Extended Kalman Filter (EKF) is used, which takes stator flux, speed, and rotor position as state variables, the stator voltage and current as input and output variables. The experiments show that the method can effectively estimate the rotor position. However, the calculation of this algorithm is complicated, and the convergence of the estimation results can not be guaranteed, resulting in poor closed-loop performance and stability.

Due to the advantages of insensitivity to parameter changes and interference, fast response speed, and easy implementation, the sliding mode observer (SMO) has been continuously developed [17]–[22], and the SMO is also widely used for sensorless control of PMSM. In [23]–[25], SMO is used to estimate the rotor position, and the error feedback from the state variable is constructed by the sign function for realizing the estimation of the rotor position, which has a high dynamic response performance. However, the sign function will cause chattering of the system, and noise has a greater influence on the estimation result in steady-state, so it is necessary to design a multi-stage filter to eliminate noise. In [26]–[29], the saturation functions and special functions are used to replace the sign function, which improves the estimation performance of rotor position to a certain extent. However, these control methods mainly focus on how to improve the estimation performance of the rotor position. In order to estimate the rotor speed, in [30], the higher-order sliding mode and Luenberger observer are used to estimate the rotor speed, the experiment shows that this method can estimate the rotor speed well, but it lacks the experiment analysis of load performance. In [31], [32], the traditional FOO and PLL is used to estimate the rotor speed respectively, the experiments show that both methods can effectively estimate the rotor speed, but their dynamic response, load capacity, and stability are poor.

In order to solve the problems of slow dynamic response and weak load capacity of the traditional sensorless vector

control system mentioned above, a scheme of sensorless vector control system based on improved SMO and improved FOO is proposed, and the main contributions of this paper can be summarized as follows:

Firstly, based on the traditional SMO, an improved SMO is proposed, which has three main innovations: First, the sign function is replaced by the saturation function. Second, in order to compensate for the phase shift caused by the low-pass filter, a low-pass filter whose cut-off frequency varies with the speed is designed, and the back EMF is fed back to the mathematical model of stator current estimation. Third, based on the stability analysis of the improved SMO, the adaptive rate of the feedback gain coefficient is proposed.

Secondly, based on the traditional FOO, an improved FOO is proposed, which has two main innovations: First, the disturbance feedback matrix is introduced to improve the dynamic response performance of the estimated value. Second, the estimated load torque is feedforward compensated to the given quadrature current terminal, which improves the load capacity and anti-load disturbance ability of the system.

Finally, in order to verify the correctness and superiority of the proposed improved SMO and improved FOO, different algorithm systems are established in this paper for experimental comparison.

This paper is organized as follows: In Section II, the theoretical design and stability of improved SMO and improved FOO are analyzed respectively, and on this basis, the sensorless vector control system based on improved SMO and improved FOO is designed. In Section III, a corresponding experimental test platform is designed, and then a comparative experiment is carried out on the sensorless vector control system proposed in this paper, and the experimental results are discussed to show the correctness and effectiveness of the design in this paper. The conclusion is drawn in Section IV.

II. THE PROPOSED NEW SENSORLESS VECTOR CONTROL SYSTEM

Vector control is one of the basic control methods in the field of motor control. In [33]–[35], the basic principle of vector control is described in detail. According to the basic theory of vector control, a new sensorless vector control system based on an improved SMO and an improved FOO is established in this paper, which is shown in Fig. 1. It consists of a speed loop based on a PI regulator, a current loop based on two PI regulators, Park transforms, space vector pulse width modulation (SVPWM), three-phase inverter, IPark transforms, Clark transforms, PMSM, an improved SMO, an improved FOO, etc. The improved SMO is used to estimate the rotor position, and the improved FOO is used to estimate the rotor speed and load torque, and feed-forward the estimated value of the load torque to the given end of the quadrature current, where m is the feedforward coefficient. The design principles of the improved SMO and the improved FOO are described below, respectively.
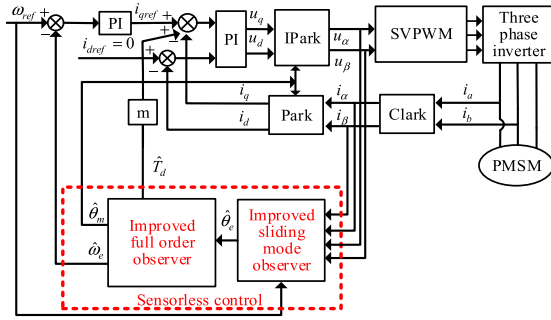
FIGURE 1. The overall block diagram of the proposed new sensorless vector control system.

A. ROTOR POSITION ESTIMATION BASED ON AN IMPROVED SMO

The PMSM model equation in the stationary reference frame is expressed as:

$$
\begin{cases}
di_\alpha/dt = -Ri_\alpha/L + (u_\alpha - e_\alpha)/L \\
di_\beta/dt = -Ri_\beta/L + (u_\beta - e_\beta)/L
\end{cases}
\tag{1}
$$

In (1), i_α, i_β, u_α, u_β are the actual current, actual voltage, respectively; R is the stator resistance, L is the stator inductance, e_α and e_β respectively represent the actual back EMF under the stationary coordinate system, the formula is as follows:

$$
\begin{cases}
e_\alpha = -k_e\omega_r \sin\theta \\
e_\beta = k_e\omega_r \cos\theta
\end{cases}
\tag{2}
$$

In (2), ω_r is the motor rotor speed, k_e is the back-EMF coefficient.

In [23], the symbolic function is used to replace the switching function to construct the traditional SMO as follows:

$$
\begin{cases}
d\hat{i}_\alpha/dt = -R\hat{i}_\alpha/L + ksgn(\hat{i}_\alpha - i_\alpha)/L \\
d\hat{i}_\beta/dt = -R\hat{i}_\beta/L + ksgn(\hat{i}_\beta - i_\beta)/L
\end{cases}
\tag{3}
$$

where, k is the sliding mode gain. sgn is the signum function.

According to (1) and (3), combined with the theory of sliding mode variable structure control, the back-EMF is obtained as follows:

$$
\begin{cases}
e_\alpha = k\,\text{sgn}\left(\hat{i}_\alpha - i_\alpha\right) \\
e_\alpha = k\,\text{sgn}\left(\hat{i}_\beta - i_\beta\right)
\end{cases}
\tag{4}
$$

After the back-EMF is estimated, the rotor position angle can be obtained by the following formula:

$$
\hat{\theta}_e = -\tan^{-1}(e_\alpha/e_\beta)
\tag{5}
$$

However, according to the test results and analysis, the back EMF obtained by (4) contains high-frequency chattering signals. Traditional SMO usually uses a low-pass filter to eliminate high-frequency chattering signal, which will bring a large phase delay. Therefore, traditional SMO has problems such as jitter, offline phase compensation, and poor estimation performance at low speeds. In order to solve these problems, the mathematical model of the traditional SMO

is improved by three core contents: A low-pass filter whose cut-off frequency can change with speed is designed, the estimated value of back EMF is introduced into the mathematical model of stator current estimation, and the adaptive rate of feedback gain coefficient is proposed.

In response to the above problems, an improved SMO based on the saturation function is designed as follows:

$$
\begin{cases}
d\hat{i}_\alpha/dt = -R\hat{i}_\alpha/L + (u_\alpha - Z_\alpha - lZ_{e\alpha})/L \\
d\hat{i}_\beta/dt = -R\hat{i}_\beta/L + (u_\beta - Z_\beta - lZ_{e\beta})/L
\end{cases}
\tag{6}
$$

where, l is the feedback gain coefficient of the control function; $Z_{e\alpha}$ and $Z_{e\beta}$ are equivalent control functions of Z_α and Z_β, which are introduced into the stator current estimation mathematical model; Z_α and Z_β are the saturation function instead of the traditional sliding mode variable structure switching function, the function curve is shown in Fig. 2.
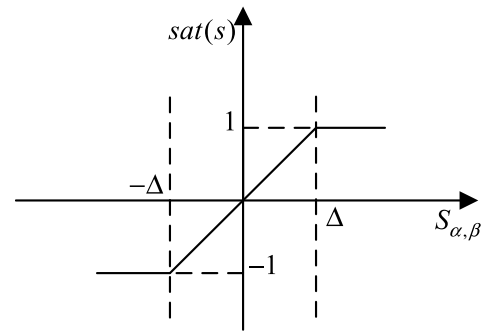

FIGURE 2. Saturation function curve.

In Fig. 2, Δ is the boundary layer and $\begin{bmatrix} S_\alpha & S_\beta \end{bmatrix}^T = \begin{bmatrix} \hat{i}_\alpha - i_\alpha \\ \hat{i}_\beta - i_\beta \end{bmatrix}$. It can be seen from the saturation function curve in Fig. 2 that this control law has two switching surfaces ($S = \Delta$, $S = -\Delta$), which is a linear function of S in the boundary layer and a continuous function on the original sliding surface $S = 0$, a variable structure system with 3 structures, defined as follows:

$$
\begin{bmatrix} Z_\alpha \\ Z_\beta \end{bmatrix} = Ksat\left(\hat{i}_s - i_s\right)
$$

$$
= K \times \begin{cases}
1 & \hat{i}_s - i_s > \Delta \\
(\hat{i}_s - i_s)/\Delta & \Delta > \hat{i}_s - i_s > -\Delta \\
-1 & -\Delta > \hat{i}_s - i_s
\end{cases}
\tag{7}
$$

where, K is the sliding mode coefficient and is greater than zero; Z_α and Z_β are control functions, defined as follows:

$$
\begin{cases}
Z_{e\alpha} = Z_\alpha\omega_c/(s + \omega_c) \\
Z_{e\beta} = Z_\beta\omega_c/(s + \omega_c)
\end{cases}
\tag{8}
$$

where, ω_c is the cutoff frequency of the low-pass filter.

From equations (1) and (6), the dynamic equation of the improved SMO can be obtained:

$$
\begin{cases}
dS_\alpha/dt = -RS_\alpha/L + (e_s - Z_s - lZ_{e\alpha})/L \\
dS_\beta/dt = -RS_\beta/L + (e_s - Z_s - lZ_{e\beta})/L
\end{cases}
\tag{9}
$$

According to the principle of SMO, the equation of motion on the sliding surface is as follows:

$$\begin{cases} S_\alpha = \hat{i}_\alpha - i_\alpha = 0 \\ S_\beta = \hat{i}_\beta - i_\beta = 0 \end{cases} \quad (10)$$

According to (9) and (10), the estimation formula of back EMF of PMSM is as follows:

$$\begin{cases} e_\alpha = Z_\alpha + lZ_{e\alpha} \\ e_\beta = Z_\beta + lZ_{e\beta} \end{cases} \quad (11)$$

After estimating the back EMF, the rotor position can be obtained according to formula (5). However, it can be seen from equation (8) that the back EMF is obtained through a low-pass filter, and there is a large phase delay, so the position information estimated by equation (5) will also have a large phase delay. Therefore, a low-pass filter whose cut-off frequency can vary with the speed in this paper is designed, and its cut-off frequency is as follows:

$$\omega_c = \omega_e / M \quad (12)$$

In (12), M is a constant (usually set to 0.2~0.5).

The rotor position of the improved SMO estimation based on rotor angle compensation is as follows:

$$\theta_e = -\tan^{-1}(e_\alpha / e_\beta) + \tan^{-1} M \quad (13)$$

Comparing with (5) and (13), it can be seen that the improved SMO introduces angular position compensation in position estimation, which can compensate for the influence of phase shift on the system.

According to the theory of sliding mode variable structure control, the stability condition of the sliding mode observer is:

$$S_{\alpha,\beta} \times \dot{S}_{\alpha,\beta} < 0 \quad (14)$$

Combining equations (9), (14) can be rewritten as:

$$S_{\alpha,\beta} \times \dot{S}_{\alpha,\beta}$$
$$= \begin{cases} \frac{1}{L_s} S_{\alpha,\beta} \left[e_{\alpha,\beta} - \left(\frac{jM+1+l}{jM+1} \right) K \right] - \frac{R}{L_s} S^2_{\alpha,\beta}, \\ \qquad\qquad S_{\alpha,\beta} > \Delta \\ \frac{1}{L_s} S_{\alpha,\beta} \left[e_{\alpha,\beta} - \left(\frac{jM+1+l}{jM+1} \right) K \right] - \frac{R}{L_s} S^2_{\alpha,\beta}, \\ \qquad\qquad S_{\alpha,\beta} < -\Delta \end{cases} \quad (15)$$

Due to $-\frac{R}{L_s} S^2_{\alpha,\beta} < 0$, when $S_{\alpha,\beta} \times \dot{S}_{\alpha,\beta}$ satisfies the following formula, the sliding mode observer satisfies the stability condition.

$$[1 + l/(jM+1)] K > |e_{\alpha,\beta}| = k_e |\omega_r| \quad (16)$$

The above formula can be rewritten as:

$$(|k_e\omega_r|/K - 1)(jM+1) < l \quad (17)$$

Since M is generally small (M = 0.2), it can be ignored. Equation (17) is simplified as follows:

$$k_e|\omega_r|/K - 1 < l \quad (18)$$

where, $K > k_e$, take $K = 1.5k_e$.

The selection of feedback gain coefficient l must meet the stability requirements of equation (18). According to (18), the adaptive law of feedback gain coefficient is proposed as follows:

$$l = |\omega_{ref}| - 1 \quad (19)$$

In (19), ω_{ref} is the given speed, during steady-state operation satisfy $\omega_{ref} = \omega_r$.

Based on the above analysis, the control block diagram of the improved SMO for rotor position estimation is shown in Fig. 3.
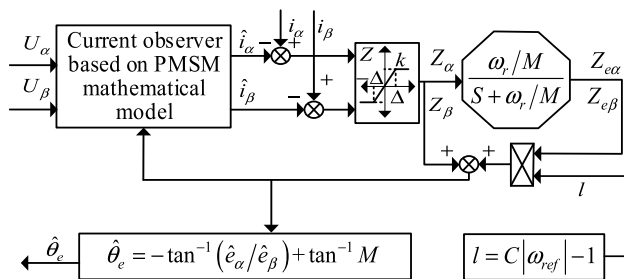

FIGURE 3. The principal block diagram of rotor position estimation based on the improved SMO.

B. ROTOR SPEED AND LOAD TORQUE ESTIMATION BASED ON AN IMPROVED FOO

Based on the rotor position estimated by the improved SMO, an improved FOO is proposed to estimate the rotor speed and load torque, which replaces the PLL or differential control used in the traditional sensorless control system [23]–[29]. In order to better understand the improvement of the FOO, the traditional FOO principle is briefly introduced firstly.

According to the state-space model of the PMSM motion equation [30], the dynamic state equation of the motor is obtained as follows:

$$\begin{cases} dx/dt = Ax + Bu \\ y = Dx \end{cases} \quad (20)$$

where: $A = \begin{bmatrix} 0 & 1 & 0 \\ 0 & -B_m/J & -1/J \\ 0 & 0 & 0 \end{bmatrix}$, $B = \begin{bmatrix} 0 \\ 1/J \\ 0 \end{bmatrix}$, $x = \begin{bmatrix} \theta_m \\ \omega_m \\ T_d \end{bmatrix}$, $D = \begin{bmatrix} 1 & 0 & 0 \end{bmatrix}$, $u = T_e$, $y = \theta_m$, ω_m is the mechanical angular velocity; θ_m is the mechanical angular position; T_e is the motor output torque; T_d is the load torque; J is the moment of inertia; B_m is the viscous damping coefficient.

The structure and parameter estimation formula of traditional FOO are obtained as follows [31]:

$$\begin{cases} d\hat{x}/dt = A\hat{x} + Bu + C(y - \hat{y}) \\ \hat{y} = D\hat{x} \end{cases} \quad (21)$$

$$\begin{cases} d\hat{\theta}_m \big/ dt = c_1 \left(\theta_m - \hat{\theta}_m \right) + \hat{\omega}_m \\ d\hat{\omega}_m \big/ dt = c_2 \left(\theta_m - \hat{\theta}_m \right) + (T_e - \hat{T}_d) \big/ J \\ d\hat{T}_d \big/ dt = c_3 \left(\theta_m - \hat{\theta}_m \right) \end{cases} \quad (22)$$

where, $\hat{x} = \begin{bmatrix} \hat{\theta}_m & \hat{\omega}_m & \hat{T}_d \end{bmatrix}^T$ is the estimated state variable, $C = \begin{bmatrix} c_1 & c_2 & c_3 \end{bmatrix}^T$ is the state feedback gain matrix.

Based on the improved SMO and traditional FOO, a sensorless vector control system is established. Different from the PLL speed estimation method [32], the traditional FOO estimates speed based on the position information estimated by the improved SMO. The experimental results show that (in the third part of the experiment), the position sensorless vector control system composed of the improved SMO and the traditional FOO compared with the improved SMO and PLL control methods has better speed dynamic response performance under no-load conditions.

However, the experimental results also show that when the load changes suddenly, the actual electromagnetic torque of the motor will respond rapidly, but the dynamic response of the load torque and speed estimated by traditional FOO is very low, and the estimated speed value differs greatly from the actual speed value, which will make the sensorless closed-loop system unstable at this moment.

In order to solve this problem, according to (21), the improved FOO based on a disturbance feedback matrix is proposed and established. The improved FOO is constructed as follows:

$$\begin{cases} d\hat{x} / dt = A\hat{x} + Bu + C(y - \hat{y}) + N \times d(y - \hat{y}) / dt \\ \hat{y} = D\hat{x} \end{cases} \quad (23)$$

where, $N = \begin{bmatrix} n_1 & n_2 & n_3 \end{bmatrix}^T$ is the feedback matrix.

According to (20) and (23), the state equation of observation deviation can be obtained:

$$\frac{d\tilde{x}}{dt} = \frac{A - CD}{I + ND} \tilde{x} \quad (24)$$

In (24), $\tilde{x} = x - \tilde{x}$ is the observation error, when $I + ND \neq 0$, that is $n_1 \neq -1$, (24) satisfies the stability requirement. The characteristic equation of (24) is obtained as follows:

$$\det \left[sI - \frac{A - CD}{I + ND} \right] = s^3 + \left(\frac{B_m}{J} + \frac{c_1 + n_2}{1 + n_1} \right) s^2$$
$$+ \frac{(Jc_2 + B_m c_1 - n_3)}{J(1 + n_1)} s - \frac{c_3}{J(1 + n_1)}$$
$$= 0 \quad (25)$$

According to the expression of the expected observer: $s^3 - (\alpha + \beta + \gamma)s^2 + (\alpha\beta + \beta\gamma + \gamma\alpha)s - \alpha\beta\gamma = 0$, suppose $B_m = 0$, and $\alpha = \beta = \gamma$, the relation between the pole and the feedback coefficient can be obtained:

$$\begin{cases} 3\alpha = -(c_1 + n_2)/(1 + n_1) \\ 3\alpha^2 = (Jc_2 - n_3)/J(1 + n_1) \\ \alpha^3 = c_3/J(1 + n_1) \end{cases} \quad (26)$$

From (23) and (26), the improved parameter estimation formula can be obtained:

$$\begin{cases} d\hat{\theta}_m \big/ dt = \hat{\omega}_m + c_1 \left(\theta_m - \hat{\theta}_m \right) + n_1 d \left(\theta_m - \hat{\theta}_m \right) \big/ dt \\ d\hat{\omega}_m \big/ dt = (T_e - \hat{T}_d) \big/ J + c_2 \left(\theta_m - \hat{\theta}_m \right) \\ \qquad + n_2 d \left(\theta_m - \hat{\theta}_m \right) \big/ dt \\ d\hat{T}_d \big/ dt = c_3 \left(\theta_m - \hat{\theta}_m \right) + n_3 d \left(\theta_m - \hat{\theta}_m \right) \big/ dt \end{cases} \quad (27)$$

Referring to the general PI regulation control theory, it can be seen that the load torque identification formula (27) of the improved FOO is similar to the general PI regulation control, c_3 and n_3 are equivalent to the integral coefficient and proportional coefficient of the PI regulator respectively. According to the traditional FOO load torque identification formula (22), it can be seen that it is only equivalent to the PI regulator with integral control. Compared with the improved FOO, the traditional method lacks the proportion link, so the dynamic response performance of the improved FOO proposed in this paper is better than the traditional method. And referring to the regulation principle of the PI regulator and in order to simplify the complexity of parameter regulation, c_3 and n_3 are set as independent regulation parameters in this paper, by substituting $c_1 = \alpha$, $n_1 = 1/\alpha$ into (26), it can be obtained that:

$$\begin{cases} c_3 = \alpha^3 J (1 + n_1) = \alpha^3 J (1 + 1/\alpha) \\ n_2 = -c_1 - 3\alpha (1 + n_1) = -4\alpha - 3 \\ n_3 = Jc_2 - 3\alpha^2 J (1 + n_1) = Jc_2 - 3\alpha^2 J (1 + 1/\alpha) \end{cases} \quad (28)$$

According to the above analysis and in combination with (28), it can be seen that the various parameters have achieved mutual adjustment, which has a certain regulating effect on the noise amplification problem caused by the position error derivative in (23). In order to further reduce the estimation error and improve the anti-interference performance of the system, the estimated load torque is used as the interference compensation signal for feed-forward compensation to the given orthogonal current terminal. According to the PMSM torque equation:

$$T_e = \frac{3}{2}P(\psi_d i_q - \psi_q i_d) \quad (29)$$

where $\psi_d = L_d i_d + \psi_f$, $\psi_q = L_q i_q$, T_e is electromagnetic torque, P is the number of pole pairs. Since the vector control strategy of $i_{dref} = 0$ is adopted in this paper, the compensation coefficients obtained from (29) is as follows:

$$m = 2 \big/ (3P\psi_f) \quad (30)$$

According to the state variables of the motor, the Lyapunov stability theory is used to analyze the stability of the observer error, and a Lyapunov function is defined as follows from the sufficient conditions for the asymptotic stability of the nonlinear system:

$$V(x) = \frac{1}{2} \left(\hat{\theta}_m^2 + \hat{\omega}_m^2 + \hat{T}_d^2 \right) \quad (31)$$

It can be seen that (31) is always greater than or equal to 0, which is positive definite. The sufficient condition for the asymptotic stability of the nonlinear system is $dV(x)/dt \leq 0$, that is, the error between the state variable and the rotor speed is gradually reduced. The specific formula is as follows:

$$\frac{dV(x)}{dt} = \hat{\theta}_m \dot{\hat{\theta}}_m + \hat{\omega}_m \dot{\hat{\omega}}_m + \hat{T}_d \dot{\hat{T}}_d \qquad (32)$$

According to the feedback gain parameter obtained in (28), the configuration of the feedback gain parameter can be transformed into the configuration of a single-pole, and the corresponding adjustment of the pole in conjunction with (27) can obtain $dV(x)/dt \leq 0$, which meets the stability condition.

According to the above analysis, the finally functional block diagram of the improved FOO is shown in Fig. 4.

FIGURE 4. The principle block diagram of the improved FOO for rotor speed and load torque estimation.

III. EXPERIMENTAL VERIFICATION

A. DESIGN OF THE EXPERIMENTAL PLATFORM

In order to verify the correctness and superiority of this method, the switchable vector control scheme of sensor control and sensorless control is designed, and its principle is shown in Fig. 5. A test platform based on the DSpace control system is designed. And the principal block diagram and physical photos of the test platform are shown in Fig. 6 and Fig. 7 respectively. They are composed of the motor (PMSM), encoder, torque and speed sensor, and load generator (PMSM), driver, current and voltage acquisition board, etc. The key parameters of the test platform are shown in Table 1.

FIGURE 5. The overall block diagram of the PMSM vector control system with sensorless control and sensor control.

FIGURE 6. The principle block diagram of the test platform.

FIGURE 7. The physical photos of the test platform.

TABLE 1. The key parameters of the test platform.

PMSM		Other Models and Parameters of the Key Equipment	
Rated speed (r/min)	2000	Load generator (PMSM)	1FK7080
Rated torque (N.m)	6	Dspace	DS1103
		Torque and speed sensor	DR-3000
Pole of pairs	4	Torque signal frequency	5KHz~15KHz
Resistance (Ω)	0.68	Speed signal frequency	1Hz~100KHz
Inductors (mH)	0.0055	Number of encoder lines	3600PPR
Total moment of inertia (kg.m²)	0.01482	Encode response frequency	125KHz
Rated voltage (V)	380	M	0.2

B. EXPERIMENTAL TEST

1) ESTIMATED PERFORMANCE TEST OF THE OBSERVER

In [26], the position estimation performance of the sensorless vector control system based on the improved SMO and PLL is tested and analyzed. The experiments show that the improved SMO proposed in this paper effectively weakens the chattering problem of the traditional SMO, and the estimated rotor position at low speed can effectively track the actual rotor position. However, the speed estimation performance, dynamic response, and load capacity are not analyzed in detail. Therefore, in order to analyze the speed estimation performance, dynamic response performance and load capacity of the sensorless vector control system designed in this paper, the following experimental comparisons are carried out respectively.

Firstly, in order to analyze the speed estimation performance of sensorless vector control system composed of improved SMO, a sensorless vector control system is established based on improved SMO and traditional FOO. According to the position information of the improved SMO estimation, the performance of the traditional FOO and PLL speeds estimation is tested and compared.
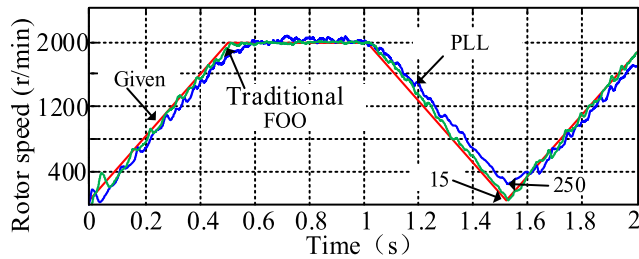

FIGURE 8. Speed estimation performance comparison between the PLL and traditional FOO.

Fig. 8 shows the speed estimation performance of the PLL and the traditional FOO when the motor operates at variable speed 15 r/min to 2000 r/min no-load condition. It can be seen from the waveform that the PLL has a higher delay in estimating the speed than the traditional FOO, the minimum speed can only run to 250 r/min due to the delay, if the sensorless closed-loop control is carried out, the dynamic response performance may be worse or even lead to system instability. The speed estimated by the traditional FOO can track the change of the given speed well and has a small delay and fluctuation, if it is used in the sensorless closed-loop control, the dynamic response performance of the system will be better. Therefore, the speed estimation performance of traditional FOO in the sensorless vector control system is better than that of PLL.

Secondly, in order to compare the estimation performance of the traditional FOO and the improved FOO, a new sensorless vector control system is established based on the improved SMO and traditional FOO, and the no-load and anti-load interference tests were carried out at a given speed of 100 r/min and 2000 r/min respectively.

The position and speed waveform estimated by the encoder(red, the same below), traditional FOO (brown), and improved FOO (blue) are obtained as shown in Fig. 9, respectively, when the given speed is 100 r/min with no-load. From the waveforms, it can be seen that the position waveform estimated by the traditional and improved observers can well follow the actual position of the motor. According to the position information obtained by the encoder, the average value of actual speed is 100.2 r/min, and the steady-state error is 0.87%. The average speed estimated by traditional FOO is 100.35 r/min, and the steady-state error is 1.54%. The average speed estimated by the improved FOO is 100.25 r/min, and the steady-state error is 0.44%, which can better track the actual speed.

Fig. 10 shows the experimental waveform of an anti-load disturbance at a given speed of 100 r/min. Due to the
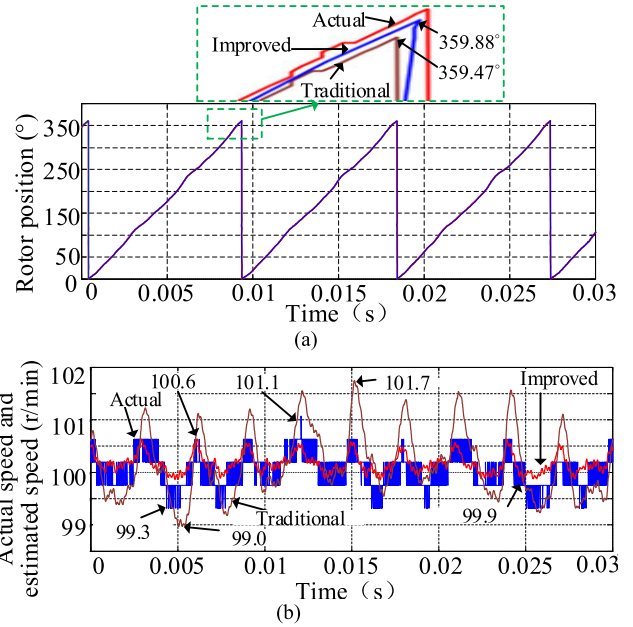

FIGURE 9. The experiment at a given speed of 100 r/min with no-load. (a) The position waveform estimated by the encoder, traditional FOO and improved FOO. (b) The speed waveform estimated by the encoder, traditional FOO, and improved FOO.
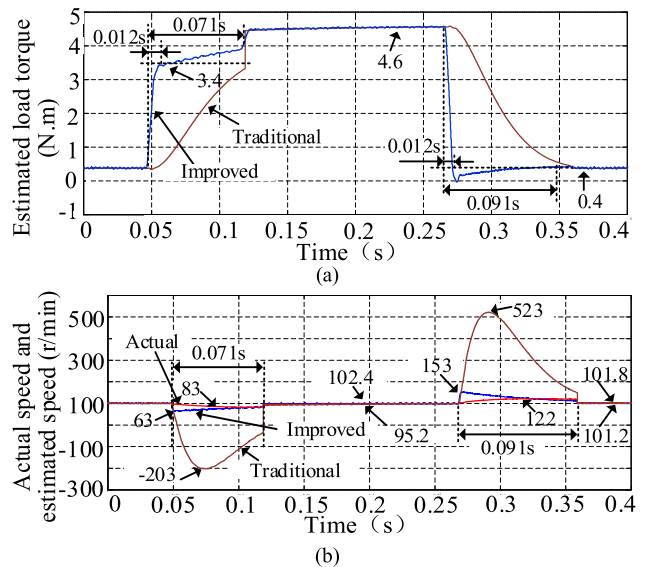

FIGURE 10. Anti-load disturbance experiment at a given speed of 100 r/min. (a) The load torque waveform estimated by the traditional FOO and improved FOO. (b) The speed waveform estimated by the encoder, traditional FOO, and improved FOO.

limitation of the test system, the maximum load torque corresponding to 100 r/min is 4.6 N.m. From the waveform in Fig. 10 (a), it can be seen that the load torque estimated by the traditional FOO rises to 3.4 N.m after 0.071 s in the process of load sudden increase. In the process of sudden load decrease, the estimated load torque value decreases to 0.4 N.m after 0.091 s. Under the same sudden load change condition, the load torque estimated by the improved FOO increased to 3.4 N.m after 0.012 s when the load was suddenly increased and decreased to 0.4 N.m after 0.012 s when the

load was suddenly unloaded. Therefore, the response performance of load torque identification of the improved observer is better than that of the traditional observer.

From the waveform in Fig. 10 (b), it can be seen that in the process of sudden load increase, the actual speed of the motor decreases from 100.4 r/min to 83 r/min, and the change value of the speed is 17.4 r/min, after 0.071 s, it recovers to 100 r/min. Under the same load change condition, the speed estimated by the traditional FOO decreases from 100.8 r/min to −203 r/min, and the change value of the speed is 303.8 r/min, after 0.071 s, it recovers to 95.2 r/min. The speed estimated by the improved FOO decreases from 101.5 r/min to 63 r/min, and the change value of the speed is 38.5 r/min and recovers to 102.4 r/min after 0.071 s.

In the process of sudden load decrease, the actual speed of the motor rises from 98.8 r/min to 122 r/min, the change value of the speed is 23.2 r/min, and it recovers to 100 r/min after 0.091 s. Under the same load change condition, the estimated speed of the traditional FOO rises from 94.7 r/min to 523 r/min, the change value of the speed is 428.3 r/min, and it recovers to 101.8 r/min after 0.091 s. The speed estimated by the improved FOO rises from 96.9 r/min to 153 r/min, the change value of the speed is 56.1 r/min, and recovers to 101.2 r/min after 0.091 s.

From the test results, when the given speed is 100r / min, the improved FOO can better track the actual speed of the motor due to the introduction of load disturbance compensation signal, and the steady-state error is small. Compared with the traditional FOO single integral link, after the improved FOO introduces the error derivative feedback term, the observation of load torque adds a proportional link to the original integral link, so the load torque estimation response is faster. And when the load changes suddenly, it has better-tracked performance for motor speed. If the traditional FOO is used to estimate the speed and perform sensorless closed-loop control, the system may become unstable when the load changes suddenly. But the speed change estimated by the improved FOO is similar to the actual speed change of the motor, so the sensorless closed-loop control can be effectively realized.

Fig. 11 is the waveform obtained from the experiment at a given speed of 2000 r/min with no-load. The observed waveform shows that the rotor position estimated by the traditional and improved observers can better follow the change of the actual position. According to the position information obtained by the encoder, the average value of actual speed is 2000.2 r/min, and the steady-state error is 0.03%. The average speed obtained by the traditional FOO is 2000.35 r/min, and the steady-state error is 0.27%. The improved FOO average speed is 2000.6 r/min, and the steady-state error is 0.12%. which is basically the same as the actual speed change of the motor.

Fig. 12. shows the experimental waveform of an anti-load disturbance at a given speed of 2000 r/min. From the waveform in Fig.12 (a), it can be seen that the load torque estimated by the traditional FOO decreases to 0.8 N.m after 0.029 s in the process of sudden load decrease, and rises
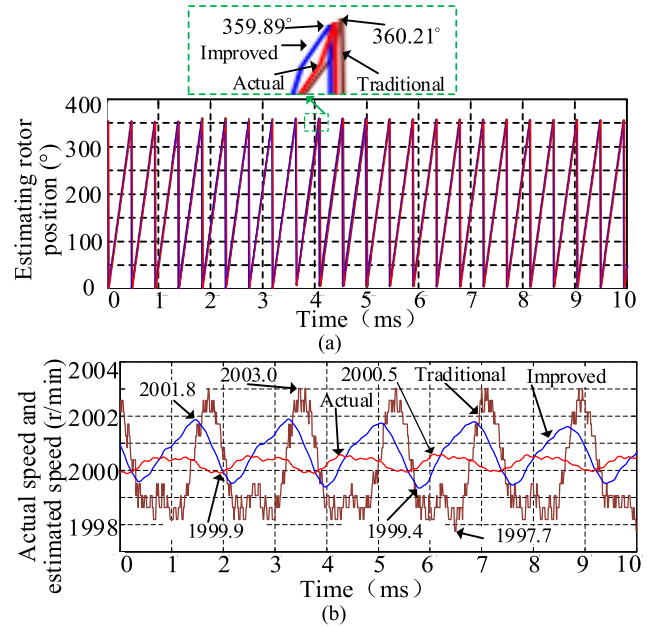

FIGURE 11. The experiment at a given speed of 2000 r/min with no-load. (a) The position waveform estimated by the encoder, traditional FOO and improved FOO. (b) The speed waveform estimated by the encoder, traditional FOO, and improved FOO.
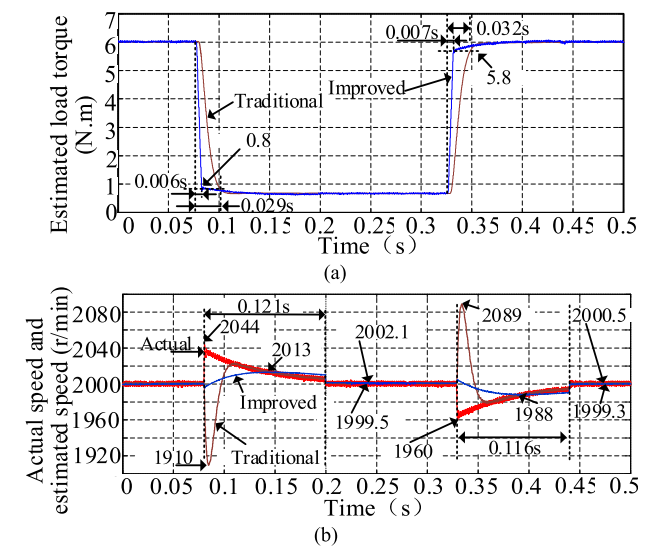

FIGURE 12. Anti-load disturbance experiment at a given speed of 2000 r/min. (a) The load torque waveform estimated by the traditional FOO and improved FOO. (b) The speed waveform estimated by the encoder, traditional FOO, and improved FOO.

to 5.8 N.m after 0.032 s in the process of sudden load increase.

Under the same sudden load change condition, the load estimated by the improved FOO decreases to 0.8 N.m after 0.006 s and rises to 5.8 N.m after 0.007 s. Therefore, the response performance of the load torque of the improved FOO is better than that of the traditional FOO.

In Fig. 12 (b), when the load decreases suddenly, the actual speed increases instantaneously from 2000 r/min to 2044 r/min. The estimated speed of the improved method

almost no change at all at the moment of load change, then increased to 2013 r/min and recovered to 1999.5 r/min after 0.121 s. However, the estimation speed of the traditional method is reduced to 1910 r/min under sudden load shedding and returns to 2002.1 r/min after 0.121 s.

When the load is suddenly increased, the actual speed decreases from 2000 r/min to 1960 r/min. The estimated speed of the improved method hardly changed at the moment of load change, then decreased to 1988 r/min, and recovered to 2000.5 r/min after 0.116 s. However, the estimated speed of the traditional method will rise to 2089 r/min instantly and returns to 1999.3 r/min after 0.116 s.

According to the above experimental results, it can be seen that at a given speed of 2000 r/min, the improved FOO can better track the actual speed of the motor due to the introduction of load disturbance compensation signal, and the steady-state error is small. compared with the traditional FOO single integral link, after the improved FOO introduces the error derivative feedback term, the observation load torque will increase the proportional link to the original integral link. Therefore, the load torque estimation response is faster, and it has better motor speed tracking performance when the load changes suddenly. If the traditional FOO is used to estimate the speed and perform sensorless closed-loop control, the system may become unstable when the load changes suddenly. But the speed change estimated by the improved FOO is similar to the actual speed change of the motor, so the sensorless closed-loop control can be effectively realized.

2) TEST OF THE INFLUENCE OF MOTOR PARAMETER CHANGES ON THE SYSTEM

In order to analyze the influence of motor parameter changes on the system, based on the method of modeling and simulation, the influence of the three motor parameters of resistance, stator inductance, and moment of inertia on the system performance is analyzed when the motor is running in the rated state.

Firstly, the influence of the stator resistance changes is analyzed. The rated value of resistance is 0.68Ω ($R = 0.68\Omega$). When the resistance changes to 0.2R, 2R, 5R, the simulation results of estimated position, speed, and load torque are shown in Fig. 13 (a), (b), and (c) respectively. By observing the waveforms in Fig.13 (a) and (b), it can be seen that when the resistance changes between 0.2R-5R, it has little influence on the estimated rotor position, and the maximum change value of position estimation is $0.12°$; when the resistance changes, the speed estimated by the improved FOO can well track the change of actual speed, and the maximum deviation of estimated speed is 1.1 r/min. It can be seen from the waveform in Fig. 13 (c) that when the resistance changes between 0.2R-5R, the estimated load torque is little affected by the resistance change, and the maximum deviation is 0.07 N.m. According to the above analysis, the resistance change has little influence on the proposed vector control system based on the improved SMO and the improved FOO.
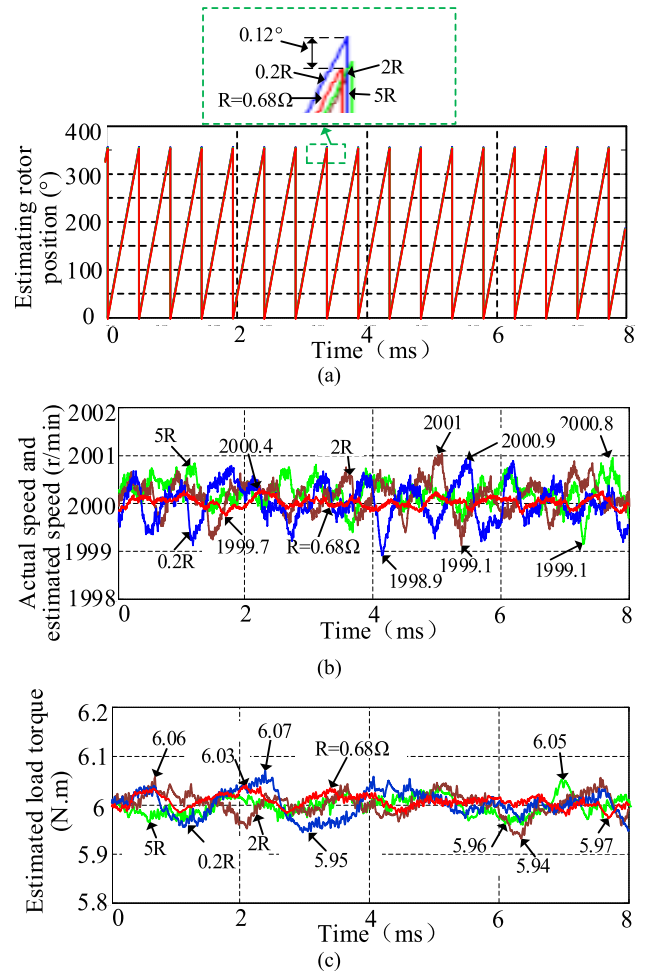

FIGURE 13. The waveform of estimated speed, position, and load torque under the different stator resistances. (a) Estimated position waveform. (b) Estimated speed waveform. (c) Load torque estimation waveform.

Secondly, the influence of stator inductance variation is analyzed. The rated value of stator inductance is 0.0055 mH (L = 0.0055 mH). When the stator inductance changes to 0.2L, 2L, 5L, the simulation results of estimated position, speed, and load torque are shown in Fig. 14 (a), (b), and (c) respectively. By observing the waveforms in Fig. 14 (a) and (b), it can be seen that when the stator inductance changes between 0.2L-5L, it has little influence on the estimated rotor position, and the maximum change value of position estimation is $0.1°$; when the stator inductance changes, the speed estimated by the improved FOO can well track the change of actual speed, and the maximum deviation of estimated speed is 1.4 r/min. It can be seen from the waveform in Fig. 14 (c) that when the stator inductance changes between 0.2L-5L, the estimated load torque is little affected by the stator inductance change, and the maximum deviation is 0.08 N.m. According to the above analysis, the stator inductance change has little influence on the proposed vector control system based on the improved SMO and the improved FOO.

Finally, the influence of the change of the moment of inertia is analyzed. The rated moment of inertia of the motor
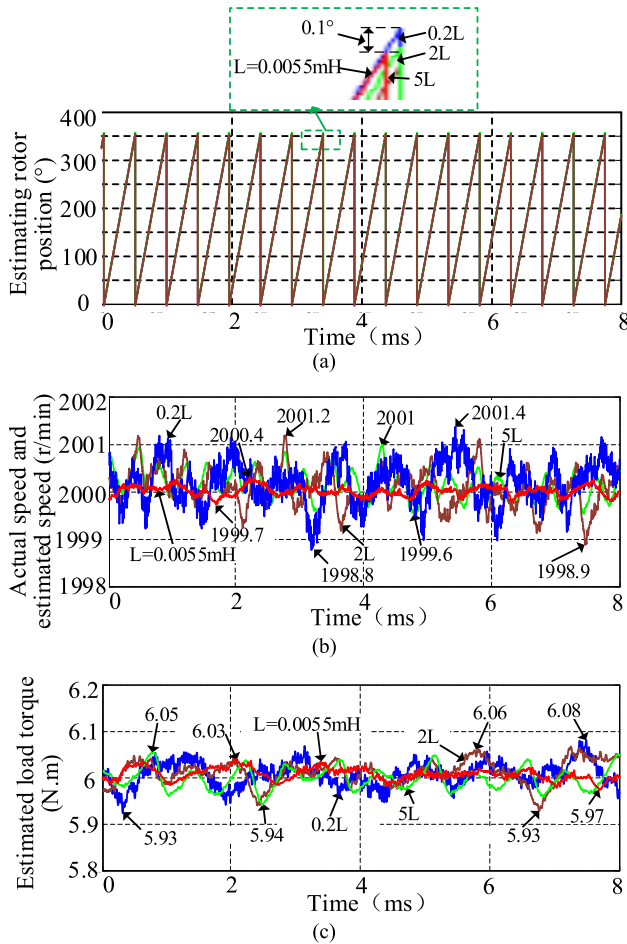
FIGURE 14. The waveform of estimated speed, position, and load torque under the different stator inductance. (a) Estimated position waveform. (b) Estimated speed waveform. (c) Load torque estimation waveform.

FIGURE 15. The waveform of estimated speed, position, and load torque under the different moment of inertia. (a) Estimated position waveform. (b) Estimated speed waveform. (c) Load torque estimation waveform.

is 0.01482 kg.m2 (J = 0.01482 kg.m2). When the moment of inertia changes to 0.2J, 2J, 5J, the simulation results of estimated position, speed, and load torque are shown in Fig. 15 (a), (b), and (c) respectively. By observing the waveforms in Fig.15 (a) and (b), it can be seen that when the moment of inertia changes between 0.2J-5J, it has little influence on the estimated rotor position, and the maximum change value of position estimation is 0.14°; when the moment of inertia changes, the speed estimated by the improved FOO can well track the change of actual speed, and the maximum deviation of estimated speed is 1.4 r/min. It can be seen from the waveform in Fig. 15 (c) that when the moment of inertia changes between 0.2J-5J, the estimated load torque is little affected by the moment of inertia change, and the maximum deviation is 0.11 N.m. According to the above analysis, the moment of inertia change has little influence on the proposed vector control system based on the improved SMO and the improved FOO.

From the above analysis, it can be seen that the changes of resistance, inductance, and moment of inertia have little influence on the proposed vector control system composed of improved SMO and improved FOO, which indicates that the control system has good robustness.
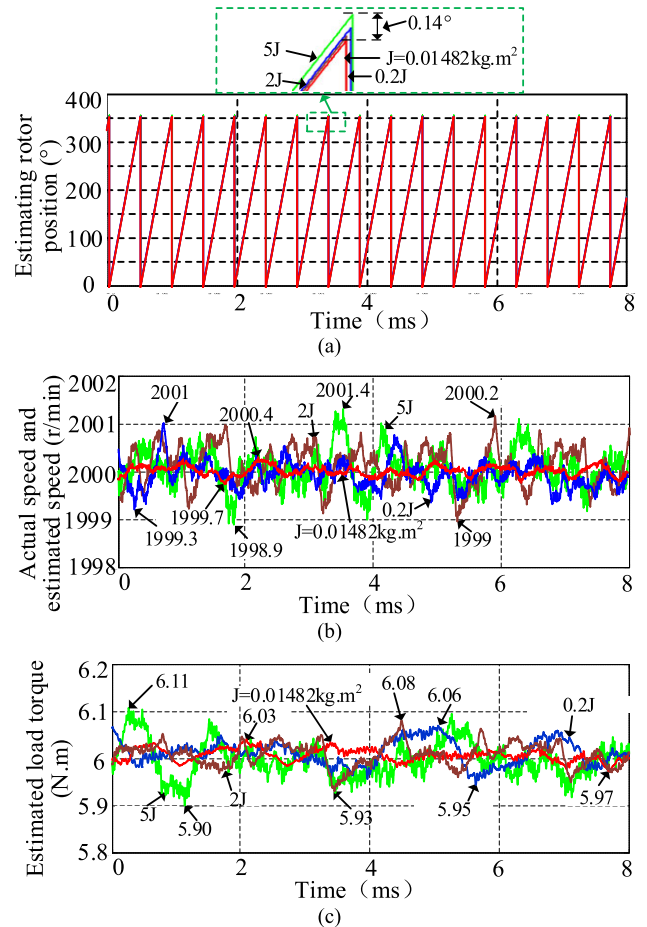
3) LOAD-CAPACITY TEST

From the previous analysis, the estimation performance of the improved FOO is better than that of the traditional FOO. In this paper, the improved SMO and the improved FOO is integrated, and the estimated load torque identification value is feedforward compensated to the given end of the quadrature axis current. Based on this, the load capacity of the sensorless vector control system is tested.

Fig. 16 is the experimental waveform obtained when the load suddenly changes when the motor is running at 100 r/min. The experimental waveforms show that when the
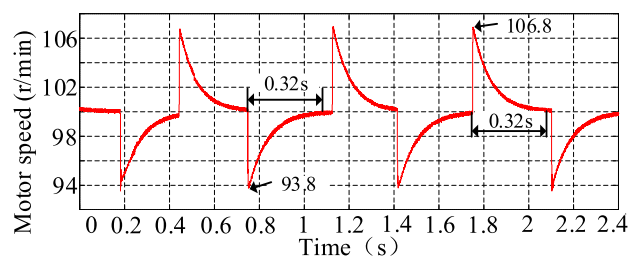

FIGURE 16. The speed waveform at a given speed of 100 r/min with full load mutation.
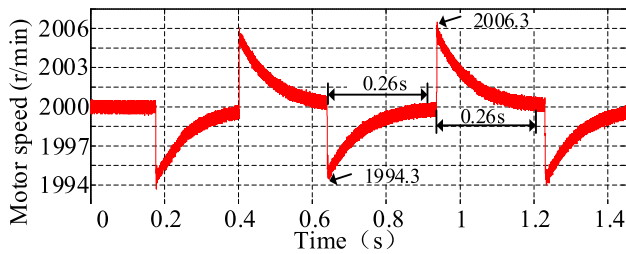
FIGURE 17. The speed waveform at a given speed of 2000 r/min with full load mutation.

load suddenly increases, the speed decreases from 100 r/min to 93.8 r/min; when the load drops suddenly, the speed rises from 100 r/min to 106.8 r/min, and the recovery time to steady-state is about 0.32 s.

Fig. 17 is the experimental waveform obtained when the load suddenly changes when the motor is running at 2000 r/min. The observed waveform shows that the speed decreases from 2000.3 r/min to 1994.3 r/min when the load suddenly increased and rises from 2000 r/min to 2006.3 r/min when the load suddenly decreased, and the recovery time to steady-state is about 0.26 s.

Therefore, the experiment proves that the sensorless vector control system designed by the proposed method has successfully realized closed-loop operation, and the system is reliable when the load suddenly changes.

IV. CONCLUSION

In order to improve the load capacity and reliability of the sensorless vector control system, an improved sensorless vector control system is proposed based on an improved SMO and an improved FOO. The improved SMO is used for estimating the rotor position, and the improved FOO is used for estimating the rotor speed and load torque. Based on the integration of these methods, a new sensorless vector control system is established finally.

The experimental results show that the dynamic follow performance of the speed of the sensorless control system designed by the improved SMO and the traditional FOO is better than that of the sensorless vector control system composed of improved SMO and PLL. But when the load changes suddenly, the dynamic response of the load torque and speed estimated by traditional FOO is very low, and the estimated speed value differs greatly from the actual speed value, which affects the reliability of the sensorless control system. While under the same load change, the load torque response of the sensorless control system designed by the improved SMO and the improved FOO is faster, and the estimated speed can better track the changing trend of the actual speed, which can achieve effective closed-loop sensorless control. Therefore, the sensorless vector control system based on improved SMO and improved FOO has a high dynamic response, load capacity, and reliability, which is more suitable for variable speed and variable load driving applications.

REFERENCES

[1] B. Yan, H. Ma, L. Zhang, W. Zheng, K. Wang, and C. Wu, "A bistable vibration isolator with nonlinear electromagnetic shunt damping," *Mech. Syst. Signal Process.*, vol. 136, Feb. 2020, Art. no. 106504.

[2] D. Ristanovic, M. Taher, T. Getschmann, and N. Bhatia, "Large synchronous motors as drivers for centrifugal compressors in LNG liquefaction plants," *IEEE Trans. Ind. Appl.*, vol. 56, no. 6, pp. 6083–6093, Nov. 2020.

[3] K.-W. Lee, S. Park, and S. Jeong, "A seamless transition control of sensorless PMSM compressor drives for improving efficiency based on a dual-mode operation," *IEEE Trans. Power Electron.*, vol. 30, no. 3, pp. 1446–1456, Mar. 2015.

[4] S. Shukla and B. Singh, "Reduced current sensor based solar PV fed motion sensorless induction motor drive for water pumping," *IEEE Trans. Ind. Informat.*, vol. 15, no. 7, pp. 3973–3986, Jul. 2019.

[5] B. Helian, Z. Chen, and B. Yao, "Precision motion control of a servomotorpump direct-drive electrohydraulic system with a nonlinear pump flow mapping," *IEEE Trans. Ind. Electron.*, vol. 67, no. 10, pp. 8638–8648, Oct. 2020.

[6] J.-W. Kwon and B.-I. Kwon, "High-efficiency dual output stator-PM machine for the two-mode operation of washing machines," *IEEE Trans. Energy Convers.*, vol. 33, no. 4, pp. 2050–2059, Dec. 2018.

[7] C. Li, G. Wang, G. Zhang, N. Zhao, and D. Xu, "Adaptive pseudorandom high-frequency square-wave voltage injection based sensorless control for SynRM drives," *IEEE Trans. Power Electron.*, vol. 36, no. 3, pp. 3200–3210, Mar. 2021.

[8] Y. Mao, Y. Du, Z. He, L. Quan, X. Zhu, L. Zhang, and Y. Zuo, "Dual quasi-resonant controller position observer based on high frequency pulse voltage injection method," *IEEE Access*, vol. 8, pp. 213266–213276, Nov. 2020.

[9] F. J. Anayi and M. M. A. Al Ibraheemi, "Estimation of rotor position for permanent magnet synchronous motor at standstill using sensorless voltage control scheme," *IEEE/ASME Trans. Mechatronics*, vol. 25, no. 3, pp. 1612–1621, Jun. 2020.

[10] Z. Wang, Z. Cao, and Z. He, "Improved fast method of initial rotor position estimation for interior permanent magnet synchronous motor by symmetric pulse voltage injection," *IEEE Access*, vol. 8, pp. 59998–60007, 2020.

[11] A. Andersson and T. Thiringer, "Motion sensorless IPMSM control using linear moving horizon estimation with luenberger observer state feedback," *IEEE Trans. Transport. Electrific.*, vol. 4, no. 2, pp. 464–473, Jun. 2018.

[12] L. He, F. Wang, J. Wang, and J. Rodriguez, "Zynq implemented luenberger disturbance observer based predictive control scheme for PMSM drives," *IEEE Trans. Power Electron.*, vol. 35, no. 2, pp. 1770–1778, Feb. 2020.

[13] S.-Y. Chen, H.-H. Chiang, T.-S. Liu, and C.-H. Chang, "Precision motion control of permanent magnet linear synchronous motors using adaptive fuzzy fractional-order sliding-mode control," *IEEE/ASME Trans. Mechatronics*, vol. 24, no. 2, pp. 741–752, Apr. 2019.

[14] A. T. Nguyen, M. S. Rafaq, H. H. Choi, and J.-W. Jung, "A model reference adaptive control based speed controller for a surface-mounted permanent magnet synchronous motor drive," *IEEE Trans. Ind. Electron.*, vol. 65, no. 12, pp. 9399–9409, Dec. 2018.

[15] Y. Shi, K. Sun, L. Huang, and Y. Li, "Online identification of permanent magnet flux based on extended Kalman filter for IPMSM drive with position sensorless control," *IEEE Trans. Ind. Electron.*, vol. 59, no. 11, pp. 4169–4178, Nov. 2012.

[16] M. Abdelrahem, C. M. Hackl, Z. Zhang, and R. Kennel, "Robust predictive control for direct-driven surface-mounted permanent-magnet synchronous generators without mechanical sensors," *IEEE Trans. Energy Convers.*, vol. 33, no. 1, pp. 179–189, Mar. 2018.

[17] Y. Hu and H. Wang, "Robust tracking control for vehicle electronic throttle using adaptive dynamic sliding mode and extended state observer," *Mech Syst. Signal Process.*, vol. 135, pp. 1–18, Jan. 2020.

[18] K. Shao, J. Zheng, K. Huang, H. Wang, Z. Man, and M. Fu, "Finitetime control of a linear motor positioner using adaptive recursive terminal sliding mode," *IEEE Trans. Ind. Electron.*, vol. 67, no. 8, pp. 6659–6668, Aug. 2020.

[19] S. He, J. Song, and F. Liu, "Robust finite-time bounded controller design of time-delay conic nonlinear systems using sliding mode control strategy," *IEEE Trans. Syst., Man, Cybern. Syst.*, vol. 48, no. 11, pp. 1863–1873, Nov. 2018.

[20] Y. Hu, H. Wang, S. He, J. Zheng, Z. Ping, K. Shao, Z. Cao, and Z. Man, "Adaptive tracking control of an electronic throttle valve based on recursive terminal sliding mode," *IEEE Trans. Veh. Technol.*, vol. 70, no. 1, pp. 251–262, Jan. 2021, doi: 10.1109/TVT.2020.3045778.

[21] S. He, W. Lyu, and F. Liu, "Robust H∞ sliding mode controller design of a class of time-delayed discrete conic-type nonlinear systems," *IEEE Trans. Syst., Man, Cybern. Syst.*, vol. 51, no. 2, pp. 885–892, Feb. 2021, doi: 10.1109/TSMC.2018.2884491.

[22] R. Nie, S. He, F. Liu, and X. Luan, "Sliding mode controller design for conic-type nonlinear semi-Markovian jumping systems of time-delayed Chua's circuit," *IEEE Trans. Syst., Man, Cybern. Syst.*, early access, May 15, 2019, doi: 10.1109/TSMC.2019.2914491.

[23] L. Sheng, W. Li, Y. Wang, M. Fan, and X. Yang, "Sensorless control of a shearer short-range cutting interior permanent magnet synchronous motor based on a new sliding mode observer," *IEEE Access*, vol. 5, pp. 18439–18450, Aug. 2017.

[24] A. K. Junejo, W. Xu, C. Mu, M. M. Ismail, and Y. Liu, "Adaptive speed control of PMSM drive system based a new sliding-mode reaching law," *IEEE Trans. Power Electron.*, vol. 35, no. 11, pp. 12110–12121, Nov. 2020.

[25] Z. Ma and X. Zhang, "FPGA implementation of sensorless sliding mode observer with a novel rotation direction detection for PMSM drives," *IEEE Access*, vol. 6, pp. 55528–55536, Sep. 2018.

[26] W. Lu, Y. Hu, X. Du, and W. Huang, "Sensorless vector control using a novel sliding mode observer for PMSM speed control system," *Proc. CSEE*, vol. 30, no. 33, pp. 78–83, Nov. 2010.

[27] D. Liang, J. Li, R. Qu, and W. Kong, "Adaptive second-order sliding-mode observer for PMSM sensorless control considering VSI nonlinearity," *IEEE Trans. Power Electron.*, vol. 33, no. 10, pp. 8994–9004, Oct. 2018.

[28] W. Xu, A. K. Junejo, Y. Liu, and M. R. Islam, "Improved continuous fast terminal sliding mode control with extended state observer for speed regulation of PMSM drive system," *IEEE Trans. Veh. Technol.*, vol. 68, no. 11, pp. 10465–10476, Nov. 2019.

[29] C. Gong, Y. Hu, J. Gao, Y. Wang, and L. Yan, "An improved delay-suppressed sliding-mode observer for sensorless vector-controlled PMSM," *IEEE Trans. Ind. Electron.*, vol. 67, no. 7, pp. 5913–5923, Jul. 2020.

[30] S. K. Kommuri, S. B. Lee, and K. C. Veluvolu, "Robust sensors-fault-tolerance with sliding mode estimation and control for PMSM drives," *IEEE/ASME Trans. Mechatronics*, vol. 23, no. 1, pp. 17–28, Feb. 2018.

[31] T. Tuovinen, M. Hinkkanen, L. Harnefors, and J. Luomi, "Comparison of a reduced-order observer and a full-order observer for sensorless synchronous motor drives," *IEEE Trans. Ind. Appl.*, vol. 48, no. 6, pp. 1959–1967, Nov. 2012.

[32] C. Lascu and G.-D. Andreescu, "PLL position and speed observer with integrated current observer for sensorless PMSM drives," *IEEE Trans. Ind. Electron.*, vol. 67, no. 7, pp. 5990–5999, Jul. 2020.

[33] Y. Zhang, L. Huang, D. Xu, J. Liu, and J. Jin, "Performance evaluation of two-vector-based model predictive current control of PMSM drives," *Chin. J. Elect. Eng.*, vol. 4, no. 2, pp. 65–81, Jun. 2018.

[34] S. Niu, Y. Luo, W. Fu, and X. Zhang, "An indirect reference vector-based model predictive control for a three-phase PMSM motor," *IEEE Access*, vol. 8, pp. 29435–29445, 2020.

[35] W. Wang, H. Yan, Y. Xu, J. Zou, X. Zhang, W. Zhao, G. Buticchi, and C. Gerada, "New three-phase current reconstruction for PMSM drive with hybrid space vector pulsewidth modulation technique," *IEEE Trans. Power Electron.*, vol. 36, no. 1, pp. 662–673, Jan. 2021.

WENQI LU (Member, IEEE) received the B.S. degree from Zhejiang Ocean University, Hangzhou, China, in 2005, and the Ph.D. degree from the Nanjing University of Aeronautics and Astronautics, Nanjing, China, in 2011.

From 2014 to 2017, he was a Postdoctoral Researcher with the Department of Electrical Engineering, Zhejiang University. From 2017 to 2018, he was a Guest Researcher with the Department of Energy Technology, Aalborg University. He is currently an Associate Professor with the Faculty of Mechanical Engineering and Automation, Zhejiang Sci-Tech University. His current research interests include the control of electric machines and mechatronic systems and its application in robot and intelligent manufacturing equipment.

DONGYANG ZHENG received the B.S. degree in measurement and control technology and instrument from Pingdingshan University, in 2018. He is currently pursuing the master's degree in control science and engineering from Zhejiang Sci-Tech University, China. His research interests include vector control for synchronous reluctance motor and the algorithm research of synchronous motor and permanent magnet AC motor control systems.

YUJUN LU received the B.S. degree from Liaoning Technical University, Liaoning, China, in 2002, and the Ph.D. degree from Zhejiang University, Hangzhou, China, in 2007.

From 2011 to 2012, he was a Visiting Scholar with the FAMU-FSU College of Engineering, Florida State University. He is currently a Professor and the Assistant Dean with the Faculty of Mechanical Engineering and Automation, Zhejiang Sci-Tech University. His current research interests include the mechatronic systems digital design and manufacturing and its application in intelligent manufacturing equipment.

KAIYUAN LU (Member, IEEE) received the B.S. and M.S. degrees from Zhejiang University, Hangzhou, China, in 1997 and 2000, respectively, and the Ph.D. degree from Aalborg University, Aalborg, Denmark, in 2005.

In 2005, he became an Assistance Professor with the Department of Energy Technology, Aalborg University, where he has been an Associate Professor, since 2008. His research interests include the design of permanent magnet machines, FEM analysis, and control of permanent magnet machines.

LIANG GUO received the master's degree from Shandong University, Jinan, China, in 2003, and the Ph.D. degree from Zhejiang University, Hangzhou, China, in 2006.

In 2006, she was a Visiting Scholar with the Power Electronics and Machines Group, The University of Nottingham, Nottingham, U.K. She is currently an Associate Professor with the Faculty of Mechanical Engineering and Automation, Zhejiang Science and Technology University, Hangzhou. Her current research interests include electromagnetic analysis and optimization of the electrical machine, in particular, in permanent magnet machines.

WEICAN YAN received the B.S. and M.S. degrees from Zhejiang University, Hangzhou, China, in 1990 and 2005, respectively, where he is currently pursuing on-the-job Ph.D. degree.

In 1990, he was the Technical Director with Wolong Electric Group Company Ltd., China, working on the motor control technology and product development. His research interests include the design and application of high-efficiency motor, and drive and motor systems.

JIAN LUO received the bachelor's degree in mechanical design manufacture and automation from Hangzhou Dianzi University, Hangzhou, China, in 2007. He is currently an Mechanical Expert with Maider Medical Industrial Equipment Company Ltd., China. His current research interest includes medical disposable automatic assembly equipment.

● ● ●